

1 Visual proteomics using whole-lamella 2D template matching

2

3 This manuscript (permalink) was automatically generated from jojoelfe/deco_lace_template_matching_manuscript@2d0a9a5
4 on March 30, 2022.

5 **Authors**

- 6 • **Johannes Elferich**  0000-0002-9911-706X ·  jojoelfe RNA Therapeutic Institute, UMass Chan Medical
7 School; HHMI
- 8 • **Nikolaus Grigorieff**  0000-0002-1506-909X ·  nikogrigorieff RNA Therapeutic Institute, UMass Chan
9 Medical School; HHMI

10 **Abstract**

11 Localization of biomolecules inside a cell is an important goal of biological imaging. Fluorescence microscopy
12 can localize biomolecules inside whole cells and tissues, but its ability to count biomolecules and accuracy of the
13 spatial coordinates is limited by the wavelength of visible light. Cryo-electron microscopy (cryo-EM) provides highly
14 accurate position and orientation information of biomolecules but is often confined to small fields of view inside
15 a cell, limiting biological context. In this study we use a new data-acquisition scheme called “Defocus-Corrected
16 Large-Area cryo-EM” (DeCo-LACE) to collect high-resolution cryo-EM data over entire sections (100 – 200 nm thick
17 lamellae) of neutrophil-like mouse cells, representing roughly 1% of the total cellular volume. We use 2D template
18 matching (2DTM) to determine localization and orientation of the large ribosomal subunit in these sections, detect
19 bound small ribosomal subunits and assign ribosomes to polysomes based on their relative orientations to each
20 other. These data provide “maps” of translational activity across sections of mammalian cells. This new high-
21 throughput cryo-EM data collection approach together with 2DTM will advance visual proteomics and complement
22 other single-cell “omics” techniques, such as flow-cytometry and single-cell sequencing.

23 **Introduction**

24 A major goal in understanding cellular processes is the knowledge of the amounts, location, interactions, and
25 conformations of biomolecules inside the cell. This knowledge can be obtained by approaches broadly divided into

26 label- and label-free techniques. In label-dependent techniques a probe is physically attached to a molecule of
27 interest that is able to detected with a high signal-to-noise signal, such as a fluorescent molecule. In label-free
28 techniques the physical properties of molecules themselves are used for detection. An example for this is proteomics
29 using mass-spectrometry [1]. The advantage of label-free techniques is that they can provide information over
30 thousands of molecules, while label-techniques offer highly specific information for a few molecules. Especially
31 spatial information can often only be achieved using label-dependent techniques, such as fluorescence microscopy
32 [2].

33 Cryo-electron microscopy has the potential to directly visualize the arrangement of atoms that compose biomole-
34 cules inside of cells, thereby allowing label-free detection with high spatial accuracy. This has been called “visual
35 proteomics” [3]. Since cryo-EM requires thin samples (<500nm), imaging of biomolecules inside cells is restricted
36 to small organisms, thin regions of cells, or samples that have been suitably thinned. Thinning can be achieved
37 either by mechanical sectioning [4] or by milling using a focused ion beam (FIB) [5]. his complex workflow leads to
38 a low throughput of cryo-EM imaging of cells and is further limited by the fact that at the required magnifications,
39 typical fields of view (FOV) are very small compared to mammalian cells, and the FOV achieved by label-techniques
40 such as fluorescence light microscopy. The predominant cryo-EM technique for the localization of biomolecules of
41 defined size and shape inside cells is cryo-electron tomography [6]. However, the requirement of a tilt series at every
42 imaged location and subsequent image alignment, severely limits the throughput for molecular localization.

43 An alternative approach is to identify molecules by their structural “fingerprint” in single projection using “2D
44 template-matching” (2DTM) [7,8,9]. In this method a 3D model of a biomolecule is used as a template to find 2D
45 projections that match the molecules visible in the electron micrographs. This method requires a projection search
46 on a fine angular grid, and the projections are used to find local cross-correlation peaks with the micrograph. Since
47 the location of a biomolecule in the z-direction causes predictable aberrations to the projection image, this method
48 can be used to calculate complete 3D coordinates and orientations of a biomolecule in a cellular sample [8]

49 Hematopoiesis is the process of generating the various cell types of the blood in the bone marrow. Disregulation
50 of the process results in diseases like leukemia. Understanding how hematopoietic stem and progenitor cells are
51 programmed to diffferentiate to the appropriate cell type would be provide new insight how hematopoiesis can be
52 misregulated. Of special interest is the regulation of translation during hematopoiesis. This is exemplified by the
53 observation that genetic defects in the ribosome machinery often leads to hematopoietic disease[10]. As such direct
54 quantification of ribosome location, number and conformational states could lead to new insight into hematopoietic
55 disease [11].

56 Here we apply 2D-template matching of ribosomes to cryo-FIB milled neutrophil-like murine cells [12]. To in-
57 crease the amount of collected data and to provide unbiased sampling of the whole lamella, we devised a new
58 data-acquisition scheme, Defocus-corrected large area cryo-electron microscopy (DeCo-LACE). We characterize

59 aberration cause by the used large beam-image shifts and highly focused beams and find that they can be ad-
60 equately corrected to enable ribosome detection by 2DTM. The resulting data provide a description of ribosome
61 distribution in the whole lamellae, which represent roughly 2% of the cellular volume. We find highly heterogeneous
62 density of ribosome within the cell and can identify discrete clusters of presumably translationally active ribosomes,
63 by testing for the presence of the small ribosomal subunit. The high accuracy of location and orientation of each
64 detected ribosome also allows us to cluster ribosome molecules into potential polysomes. Analysis of the throughput
65 in this method suggests that for the foreseeable future computation will be the bottleneck for visual proteomics.

66 Materials and Methods

67 Grid preparation

68 ER-HoxA9 cells were maintained in RPMI supplemented with 10% FBS, penicillin/streptomycin, SCF, and estrogen
69 [12] at 37C and 5% CO₂. 120h prior to grid freezing cells were washed twice in PBS and cultured in the same
70 medium, except without estrogen. Differentiation was verified by staining with Hoechst-dye and inspection of
71 nuclear morphology. Cells were then counted and diluted to 1^106 cells/ml. Grids (either 200 mesh copper grids,
72 with a silicone-oxide and 2um holes with a 2um spacing or 200 mesh gold grids with a thin gold film and 2 um
73 holes in 2um sapcing) were glow-discharged from both sides using a ... for 3.5 ul of cells suspension was added to
74 grids on the thin-film side and grids were automatically blotted from the back-side using a GP2 cryoplunger (Leica)
75 for ... s and rapidly plunged into liquid ethane at -185C.

76 FIB-milling

77 Grids were loaded into a Acquilos 2 FIB/SEM microscope with a stage cooled to -190C. Grids were sputter-coated
78 with platinum for 15s at 45 mA and then coated with a layer of platinum-precursor by openin the GIS-valve for
79 45s. An overview of the grid was created by montaging SEM images and isolated cells at the center of gridsquares
80 were selected for FB-milling. Lamella were generated automatically using the AutoTEM software, resulting in 6-8
81 um wide lamella with 150-200 um thickness as determined by FIB-imaging of the lamella edge.

82 Data collection

83 Grids were loaded into a Krios Titam TEM operated at 300 keV. The microscope was setup with a cross-grating grid
84 on the stageby setting the beam-diameter to 900 nm, resulting in the beam being completely visible in the camera.
85 To establish fringe-free conditions, the “Fine eucentric” procedure of serialEM was used to move a square of the
86 cross-grating grid to the eucentric position of the microscope. The effective defocus was then set to 2 um, using the
87 “autofocus” routine of serialEM. The objective focus of the microscope was changed until no fringes were visible.
88 The stage was then moved in Z until images had a apparent defocus of 2 um. The differnce in stage Z-position
89 between the eucentric and fringe-free conditions was calculate d and noted to move other areas into fringe-free

90 condition.

91 Low magnification montages were used to find lamella and lamella that were sufficiently thin and free of contamination
92 were selected for automated data collection. The corners of the lamella were manually annotated in SerialEM
93 and translated into Beam-Imageshift values using SerialEm calibration. A hexagonal patter of beam-imageshift
94 positions was calculated that covered the area between he four corners in a serpentine way, with a $\sqrt{3} * 400$ nm
95 horizontal spacing and 800 nm vertical spacing. Exposures were then taking at each position with a 30 e/A total
96 dose. After each exposure that defocus was estimated using the ctffind function of SerialEM and the focus for th
97 next exposure was corrected by the difference between the estimated focus and the desired defocus of 800 um. Also
98 after each exposure the deviation of the beam from the center of the camera was measured and corrected using the
99 “CenterBeamFrom IMage” command of SerialEM.

100 After datacollection a 20s exposure at 2250x magnification of the lamella at 200um defocus was taken for visualiza-
101 tion purposes.

102 **Data pre-processing**

103 Movies were gain-corrected and motion-corrected using a custom version of unblur. To avoid influence of the beam-
104 edge on motion-correction only a quarter of the movie in the center of the camera was considered for calculation of
105 the estimated motion. After movie frames were aligned and summed a mask for the illuminated area was calculated
106 by lowpass filtering the image at ... A, thresholding the image at 10% of the maximal value and then lowpass filtering
107 the mask at ... A. This mask was then used to replace un-illuminated area with gaussian noise, with the same mean
108 and standard deviation as the illuminated area. The contrast-transfer function (CTF) was estimated using ctffind,
109 searching between 0.02 and 2 um defocus.

110 **Template matching**

111 The search template was generated from the cryo-EM structure of the mouse large ribosomal subunit (PDB 6SWA).
112 The ... subunit was deleted from the model and the simulate program of the cisTEM suite was used to calculate an
113 density map from the atomic coordinates. The match_template program was used to search for this template in
114 the preprocessed images, using 1.5 deg angular step in out-of-plane angles and 1.0 deg in-plane. 21 defocus planes in
115 200nm steps centered around the defocus estimates by ctffind were searches. Matches were defined as peaks above
116 a threshold calulated according to ... (7.75 for most images).

¹¹⁷ Data analysis

¹¹⁸ Results

¹¹⁹ 2DTM detects large ribosomal subunits in cryo-FIB lamella of mammalian cells

¹²⁰ To test whether we could detect individual ribosomes in mammalian cells we prepared cryo-lamella of mouse
¹²¹ neutrophil-like cells. Low-magnification images of these lamellas clearly shows cellular features consistent with a
¹²² neutrophil-like phenotype, mainly a segmented nucleus and a plethora of membrane-organelles, corresponding to the
¹²³ granules and secretory vesicles of neutrophils (Fig. 1A). We then proceeded to acquire micrographs on this lamella
¹²⁴ with a defocus of 0.5-1.0 um, 30 e/A²/s exposure and 1.5 Å pixelsize. We manually selected multiple locations
¹²⁵ in the lamella and focused using standard low-dose techniques where focusing is performed on a sacrificial area.
¹²⁶ The resulting micrographs showed no signs of crystalline ice and had Thon-rings to resolution, indicating successful
¹²⁷ vitrification.

¹²⁸ We used an atomic model of the 60S mouse ribosomal subunit (6SWA) for 2D template matching. In a subset
¹²⁹ of images the distribution of cross-correlation scores significantly exceeded the distribution expected from non-
¹³⁰ significant matching. In the resulting scaled maximum-intensity maps, clear peaks with SNR thresholds up to 10
¹³¹ were apparent (Fig. S1A). By using the criterion described by for thresholding potential matches we found that in
¹³² images of cytosolic compartments we found evidence of 10-500 ribosomes in the imaged areas. Notably we found
¹³³ no matches in images that were taken in the nuclear compartment. In the cytosolic areas we found a drastically
¹³⁴ different number of matches, In some areas we found only ~ 50 matches per image area, while in another area we
¹³⁵ found more than 500 matches . This ten-fold difference in local ribosome concentration , but we realized that current
¹³⁶ data acquistion protocols are limited in that only a small area of the lamella is actually imaged and, due to the
¹³⁷ manual selection of acquisition positions based on the overview image, might be biased towards cellular region that
¹³⁸ appear appealing to the experimentalist. We therefore set out to collect cryo-EM data for 2DTM from mammalian
¹³⁹ lamella in a high-throughput unbiased fashion. #### DECO-LACE for 2D imaging of whole lamella

¹⁴⁰ In order to obtain high-resolution data for complete lamella we used a new approach for data collection. This
¹⁴¹ approach uses three key strategies: (1) ensures that every electron that exposes the sample is collected on the
¹⁴² camera (2) uses beam-image shift to precisely and quickly raster the surface of the lamella and (3) uses a focusing
¹⁴³ strategy that does not rely on a sacrificial area.

¹⁴⁴ To ensure that every electron exposing the sample was captured by the detector, we focused the electron beam so
¹⁴⁵ that the entire beam was placed on the detector. During canonical low-dose imaging the microscope is configured
¹⁴⁶ so that the focal plan is identical to the eucentric plane of the specimen stage. This leaves the C2 aperture out
¹⁴⁷ of focus, resulting in ripples at the edge of the beam (Figure 2B). While these ripples are low-resolution features
¹⁴⁸ that might not interfere with 2D template matching, which is designed to be robust to low-resolution noise, we also

¹⁴⁹ tested collecting data under a condition where the C2 aperture is in focus (Figure 2C).

¹⁵⁰ We then centered a lamella under the electron beam and used beam-image shift of the microscope to systematically
¹⁵¹ raster the whole surface of the lamella in a hexagonal pattern. Instead of focusing in a sacrificial area, we determined
¹⁵² the defocus after every exposure using a routine implemented in SerialEM modeled after CTFFind. The focus was
¹⁵³ then adjusted based on the difference between desired and measured defocus. Since we used a serpentine pattern
¹⁵⁴ for data collection every exposure is close to the previous exposure making drastic changes in the defocus unlikely.
¹⁵⁵ Furthermore we started our acquisition pattern on the platinum deposition edge, so the initial exposure where the
¹⁵⁶ defocus was not yet adjusted did not contain any biologically relevant information.

¹⁵⁷ We used this strategy to collect data on 8 lamella, 4 using the eucentric focus condition and 4 using the fringe-free
¹⁵⁸ condition. We were able to highly consistently collect data with a defocus of 8 um (Figure 2D), both in the eucentric
¹⁵⁹ focus and fringe-free focus condition. Together with the nominal defocus of the microscope this data results in a
¹⁶⁰ topological map of the lamella. To ensure that data was collected consistently, we mapped defocus values as a
¹⁶¹ function of the applied Beam-image shift (Figure 2E). This demonstrated that the defocus was consistent over the
¹⁶² lamella, with outliers only at isolated images and in images containing contamination. We also plotted the measure
¹⁶³ objective astigmatism of the lamella and found that it varies with the applied Beam-image shift, become more
¹⁶⁴ astigmatic mostly due to beam-image shift in the X direction. While approaches exist to correct this during the
¹⁶⁵ data-collection, we opted to not use these mechanism for these early experiments and instead rely on computational
¹⁶⁶ correction of these aberrations in order to characterize them.

¹⁶⁷ **2D-Template matching of cryo-EMILIA data reveals ribosome distribution**

¹⁶⁸ We developed customized preprocessing protocol to images obtained by cryo-EMILIA to enable their use for 2D-
¹⁶⁹ template matching. First we restricted calculation of cross-correlation coefficients between individual movie frames
¹⁷⁰ to the central portion of the image to prevent artifacts from the beam edges on estimation of motion. Then we
¹⁷¹ calculated a mask that defined the illuminated area of the micrographs and used it to fill non-illuminated areas with
¹⁷² gaussian noise, matching mean and standard deviation to the illuminated signal (Figure 3A). The so processed
¹⁷³ images were suitable for 2D-template matching and we were able to obtain matches with the same model used
¹⁷⁴ for the data in Figure 1.

¹⁷⁵ **Quantitative analysis of translation activity**

¹⁷⁶ **Discussion**

- ¹⁷⁷ • Elizabeth Wright and Grant Jensen Montage tomography papers
- ¹⁷⁸ • Waffle method for higher throughput, automation of fib-milling

- 179 • Throughput and bottlenecks
 180 • Visual proteomics
 181 • Granules containing ribosomes?
 182 • Threshold implications (no matches on most images)

183 **Figures**

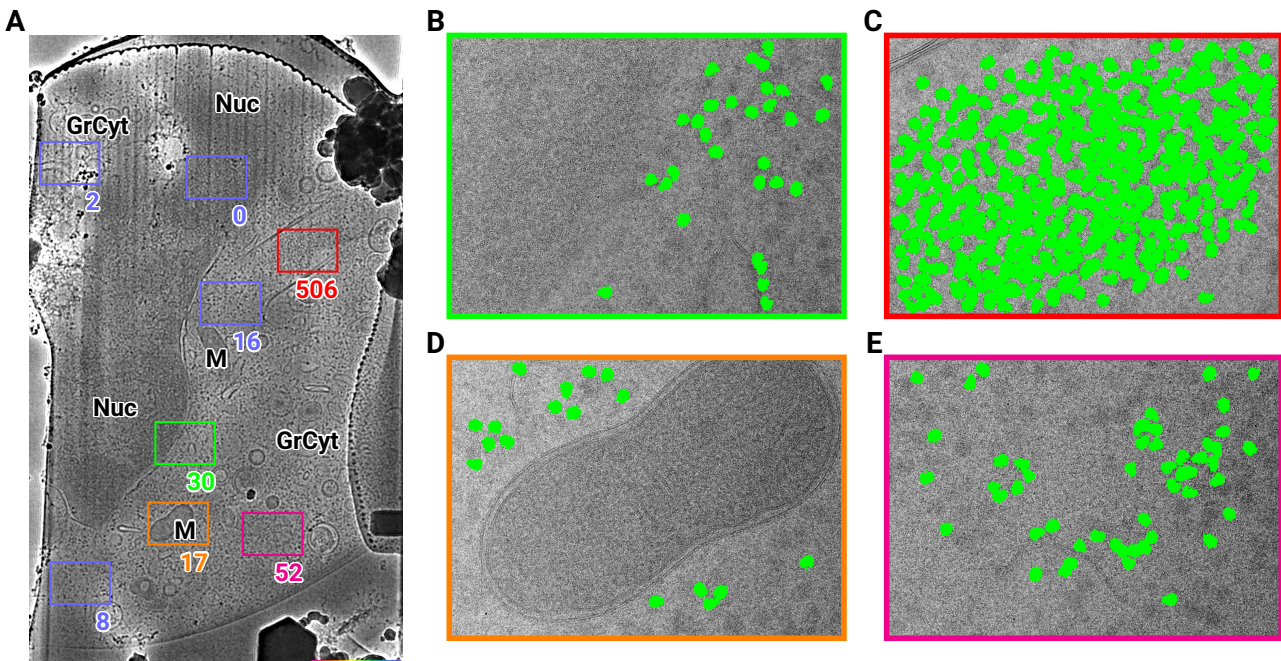


Figure 1: 2D template matching of the large subunit of the ribosome in fib-milled neutrophil-like cells (A) Overview image of the lamella. Major cellular regions are labeled, as Nucleus (Nuc), Mitochondria (M), and granular cytoplasm (GrCyt). FOVs where high-magnification images for template matching were acquired are indicated as boxes with the number of matches indicated on the bottom right. FOVs displayed in Panels B-E are color-coded. (B-E) FOVs with projection of ribosome LSU matches shown in green. (B) Perinuclear region, the only matches are in the cytoplasmic half. (C) Cytoplasmic region with high density of ribosomes (D) Mitochondrion, as expected there are only matches in the cytoplasmic region (E) Cytoplasm, with low density of ribosomes.

184 **References**

- 185 1. **Label-free, normalized quantification of complex mass spectrometry data for proteomic analysis** Noelle M Griffin, Jingyi Yu, Fred Long, Phil Oh, Sabrina Shore, Yan Li, Jim A Koziol, Jan E Schnitzer
Nature Biotechnology (2010-01) <https://doi.org/fshgnc> DOI: 10.1038/nbt.1592 · PMID: 20010810 · PMCID: PMC2805705

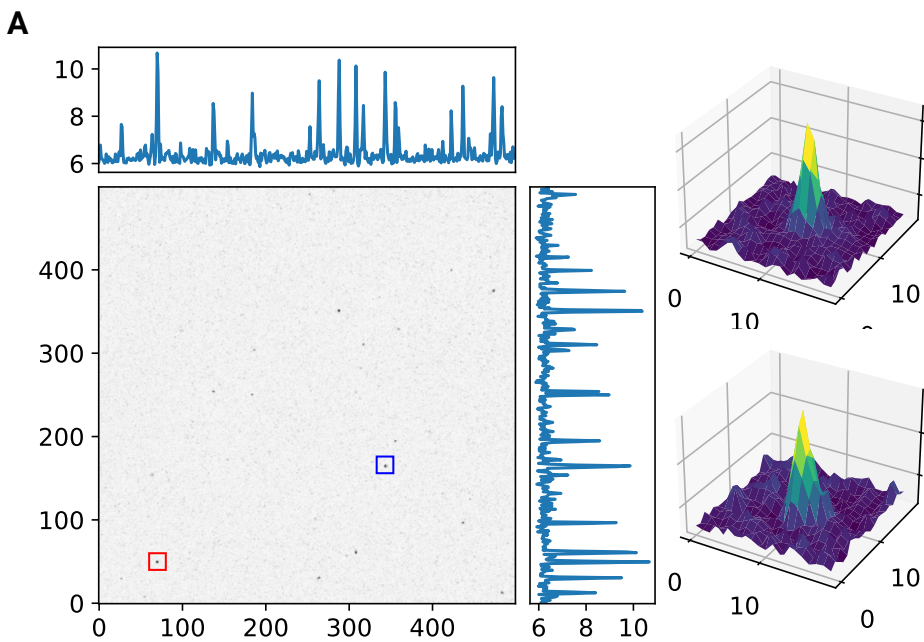


Figure S1: Maximum intensity projection cross-correlation map of micrograph shown in Figure 1

187 2. **Fluorescence microscopy** Jeff W Lichtman, José-Angel Conchello

Nature Methods (2005-11-18) <https://doi.org/bbpg4n> DOI: 10.1038/nmeth817 · PMID: 16299476

188

189 3. **A visual approach to proteomics** Stephan Nickell, Christine Kofler, Andrew P Leis, Wolfgang Baumeister

Nature Reviews Molecular Cell Biology (2006-02-15) <https://doi.org/d6d5mq> DOI: 10.1038/nrm1861 · PMID: 16482091

190

191 4. **Electron microscopy of frozen hydrated sections of vitreous ice and vitrified biological samples**

AW McDowall, J-J Chang, R Freeman, J Lepault, CA Walter, J Dubochet

Journal of Microscopy (1983-07) <https://doi.org/bdnzmv> DOI: 10.1111/j.1365-2818.1983.tb04225.x · PMID: 6350598

192

193 5. **Opening windows into the cell: focused-ion-beam milling for cryo-electron tomography**

Elizabeth Villa, Miroslava Schaffer, Jürgen M Plitzko, Wolfgang Baumeister

Current Opinion in Structural Biology (2013-10) <https://doi.org/f537jp> DOI: 10.1016/j.sbi.2013.08.006 · PMID: 24090931

194

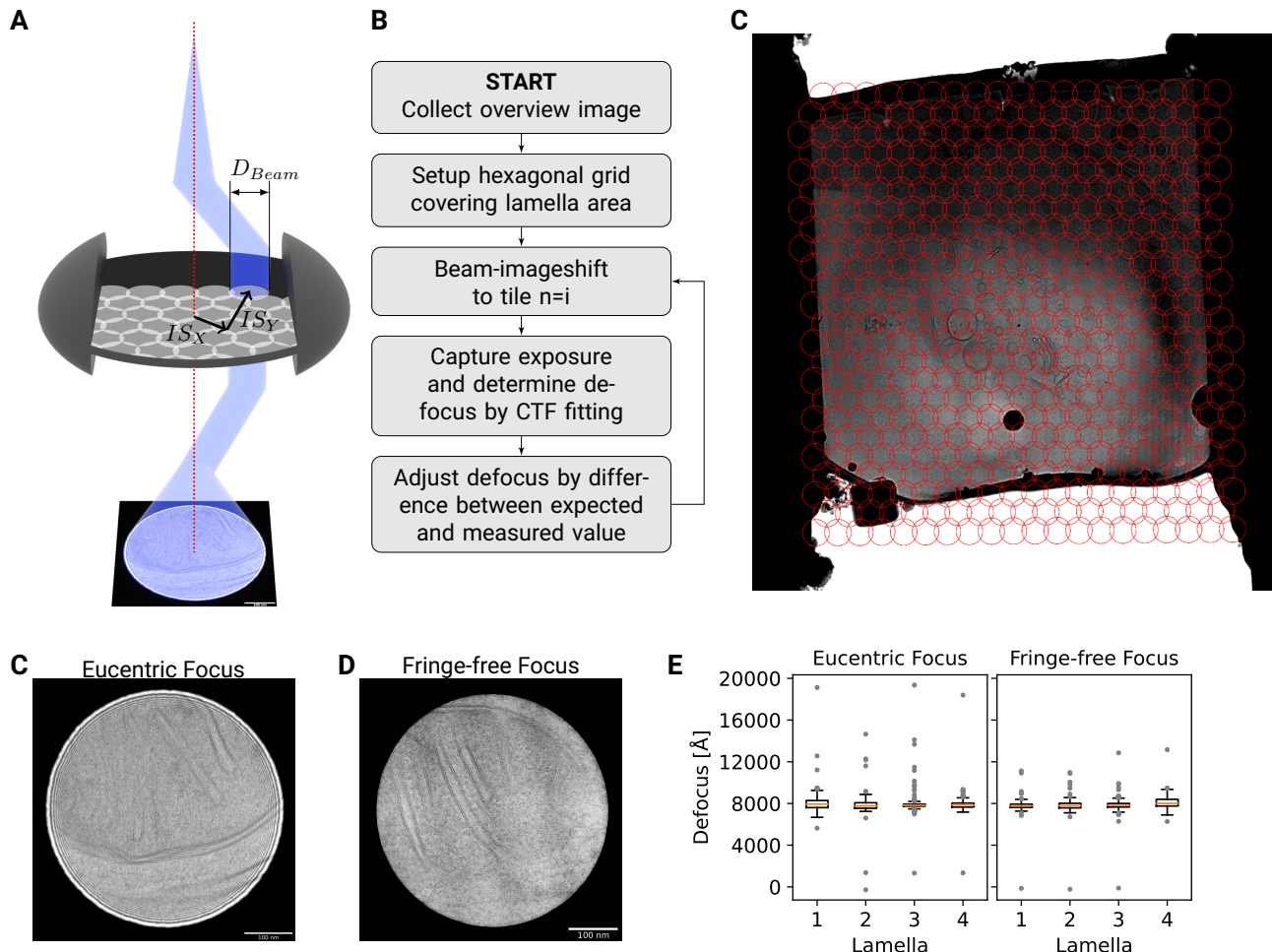


Figure 2: DeCo-LACE approach (A) Graphic demonstrating the data-collection strategy for DeCo-LACE

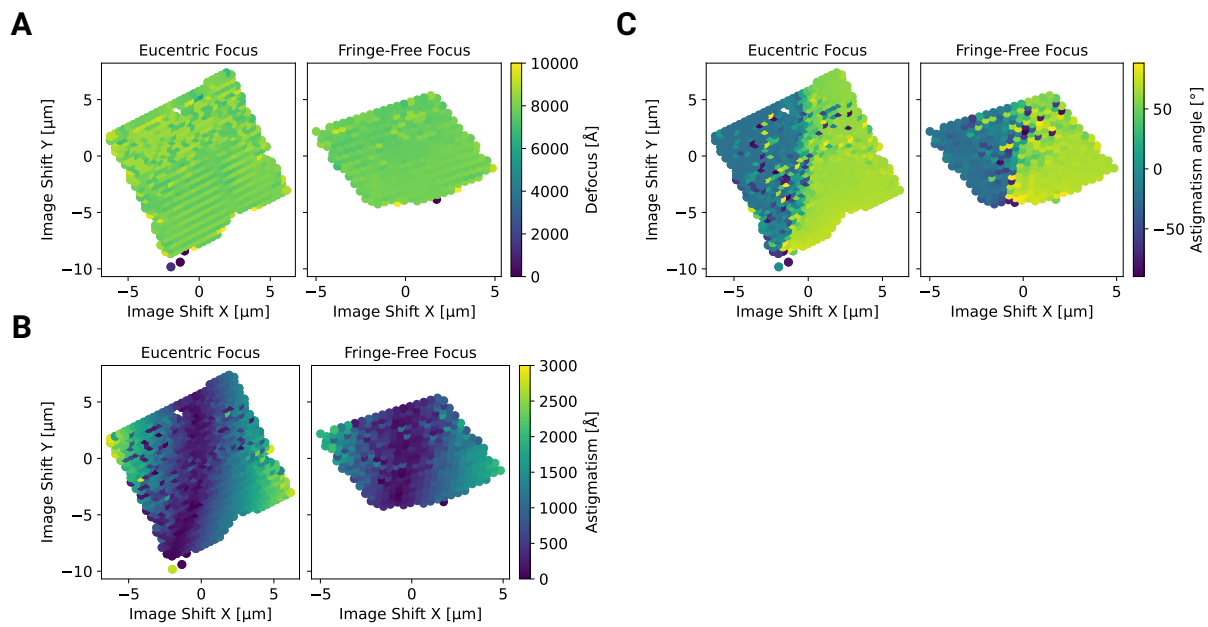


Figure 3: This is an example-figuren

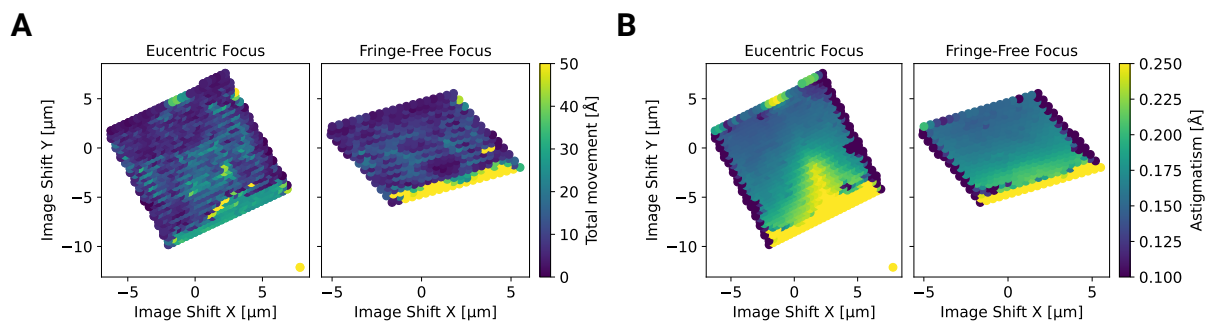


Figure 4: This is an example-figuren

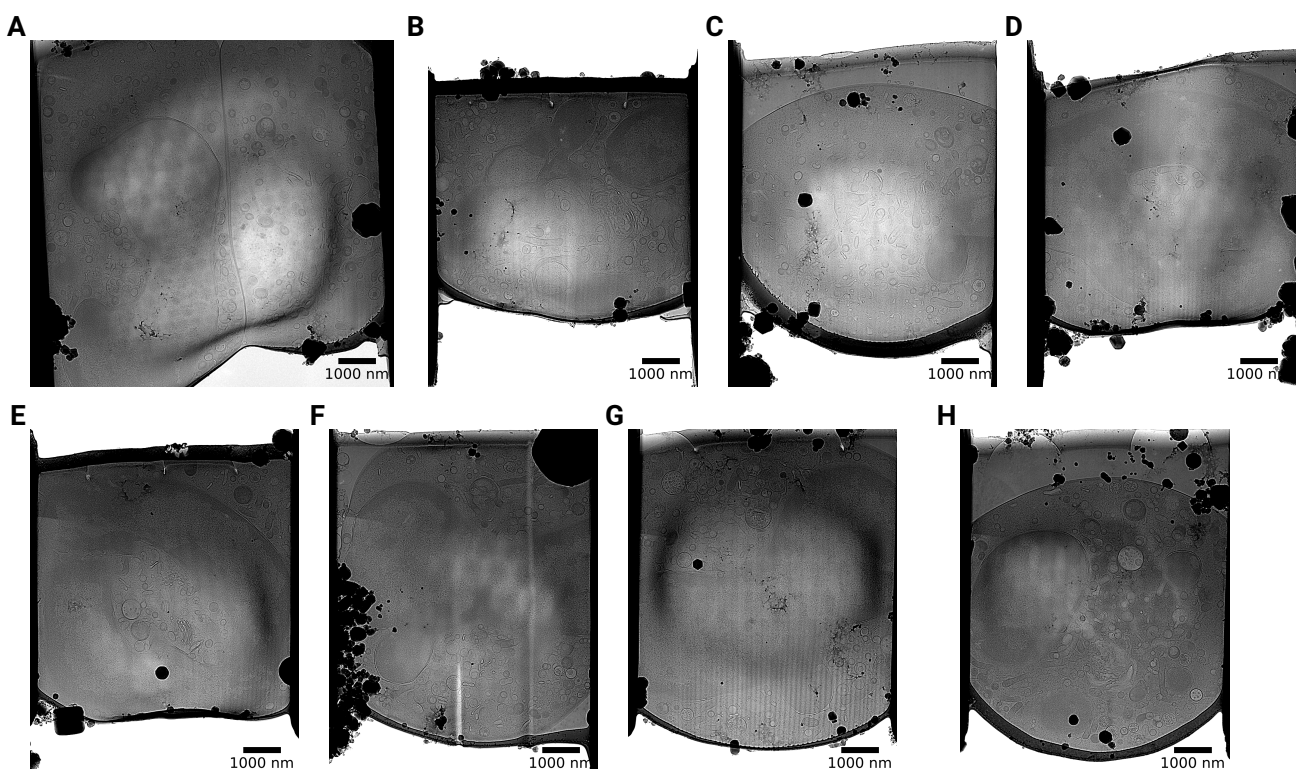


Figure 5: This is an example-figure



Figure 6: This is an example-figure

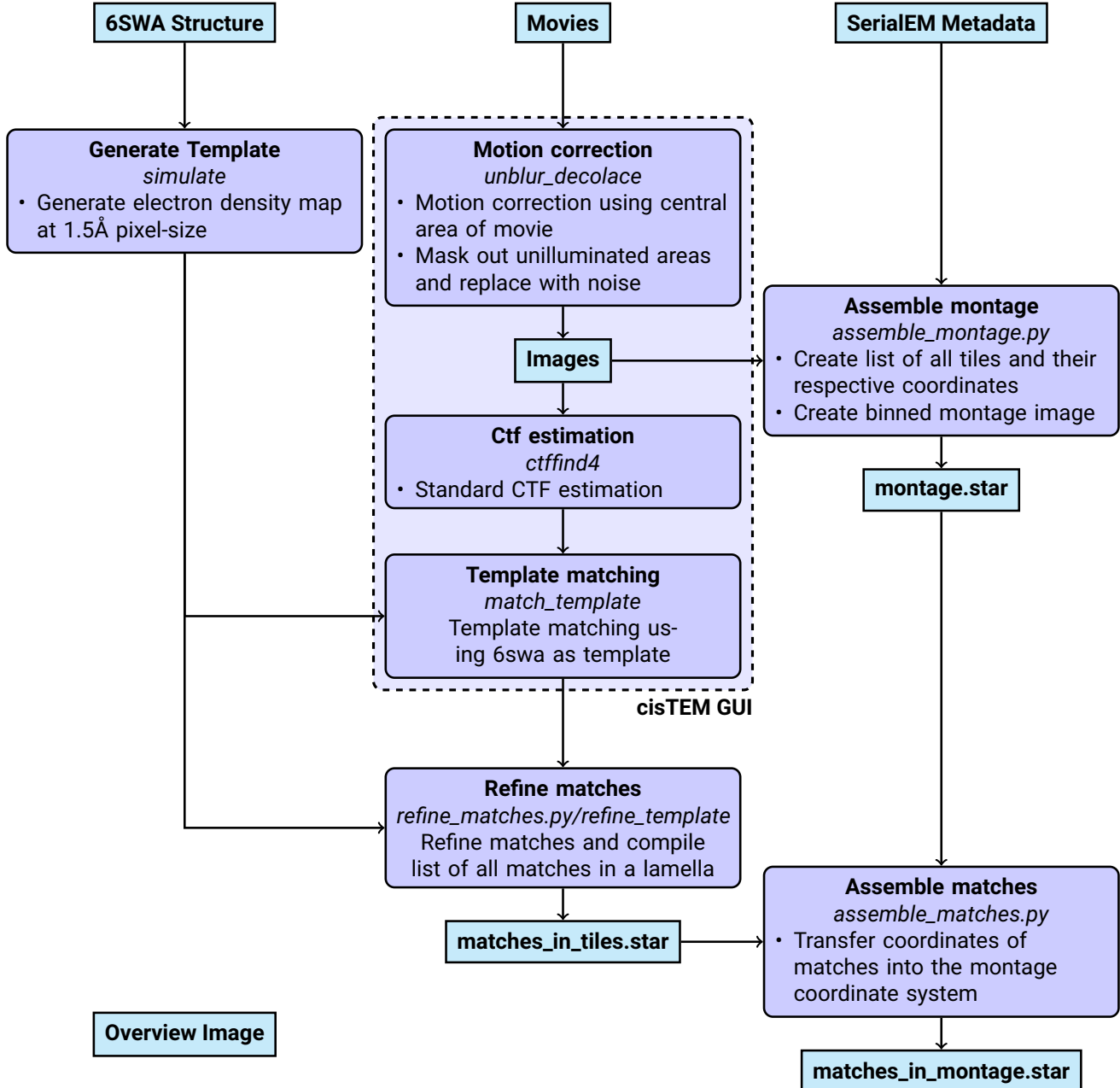


Figure 7: Workflow of DeCo-Lace processing

- 195 6. **Electron tomography of cells** Lu Gan, Grant J Jensen
Quarterly Reviews of Biophysics (2011-11-15) <https://doi.org/czj9hr> DOI: 10.1017/s0033583511000102 ·
PMID: 22082691
- 196
- 197 7. **Single-protein detection in crowded molecular environments in cryo-EM images** JPeter Rickgauer, Nikolaus Grigorieff, Winfried Denk
eLife (2017-05-03) <https://doi.org/gnq4q4> DOI: 10.7554/elife.25648 · PMID: 28467302 · PMCID: PMC5453696
- 198
- 199 8. **Label-free single-instance protein detection in vitrified cells** JPeter Rickgauer, Heejun Choi, Jennifer Lippincott-Schwartz, Winfried Denk
Cold Spring Harbor Laboratory (2020-04-24) <https://doi.org/gpbjfd> DOI: 10.1101/2020.04.22.053868
- 200
- 201 9. **Locating macromolecular assemblies in cells by 2D template matching with cisTEM** Bronwyn A Lucas, Benjamin A Himes, Liang Xue, Timothy Grant, Julia Mahamid, Nikolaus Grigorieff
eLife (2021-06-11) <https://doi.org/gkkc49> DOI: 10.7554/elife.68946 · PMID: 34114559 · PMCID: PMC8219381
- 202
- 203 10. **Hallmarks of ribosomopathies** Kim R Kampen, Sergey O Sulima, Stijn Vereecke, Kim De Keersmaecker
Nucleic Acids Research (2019-07-27) <https://doi.org/gpbjfm> DOI: 10.1093/nar/gkz637 · PMID: 31350888 · PMCID: PMC7026650
- 204
- 205 11. **Diagnostic and prognostic implications of ribosomal protein transcript expression patterns in human cancers** James M Dolezal, Arie P Dash, Edward V Prochownik
BMC Cancer (2018-03-12) <https://doi.org/gc87j9> DOI: 10.1186/s12885-018-4178-z · PMID: 29530001 · PMCID: PMC5848553
- 206
- 207 12. **Inhibition of Dihydroorotate Dehydrogenase Overcomes Differentiation Blockade in Acute Myeloid Leukemia** David B Sykes, Youmna S Kfouri, François E Mercier, Mathias J Wawer, Jason M Law, Mark K Haynes, Timothy A Lewis, Amir Schajnovitz, Esha Jain, Dongjun Lee, ... David T Scadden
Cell (2016-09) <https://doi.org/f3r5jr> DOI: 10.1016/j.cell.2016.08.057 · PMID: 27641501 · PMCID: PMC7360335